JACS
JOURNAL OF THE AMERICAN CHEMICAL SOCIETY
Article
pubs.acs.org/JACS

Activating Cobalt Nanoparticles via the Mott–Schottky Effect in Nitrogen-Rich Carbon Shells for Base-Free Aerobic Oxidation of Alcohols to Esters

Hui Su,[†] Ke-Xin Zhang,[†] Bing Zhang,[†] Hong-Hui Wang,[†] Qiu-Ying Yu,[†] Xin-Hao Li,*[,†] Markus Antonietti,[‡] and Jie-Sheng Chen[†]

[†]School of Chemistry and Chemical Engineering, Shanghai Jiao Tong University, Shanghai 200240, P. R. China

[‡]Department of Colloid Chemistry, Max-Planck Institute of Colloids and Interfaces, Wissenschaftspark Golm, 14424 Potsdam, Germany

Supporting Information

ABSTRACT: Heterogeneous catalysts of inexpensive and reusable transition-metal are attractive alternatives to homogeneous catalysts; the relatively low activity of transition-metal nanoparticles has become the main hurdle for their practical applications. Here, the *de novo* design of a Mott–Schottky-type heterogeneous catalyst is reported to boost the activity of a transition-metal nanocatalyst through electron transfer at the metal/nitrogen-doped carbon interface. The Mott–Schottky catalyst of nitrogen-rich carbon-coated cobalt nanoparticles (Co@NC) was prepared through direct polycondensation of simple organic molecules and inorganic metal salts in the presence of g-C_3N_4 powder. The Co@NC with controllable nitrogen content and thus tunable Fermi energy and catalytic activity exhibited a high turnover frequency (TOF) value (8.12 mol methyl benzoate mol^{-1} Co h^{-1}) for the direct, base-free, aerobic oxidation of benzyl alcohols to methyl benzoate; this TOF is 30-fold higher than those of the state-of-the-art transition-metal-based nanocatalysts reported in the literature. The presented efficient Mott–Schottky catalyst can trigger the synthesis of a series of alkyl esters and even diesters in high yields.

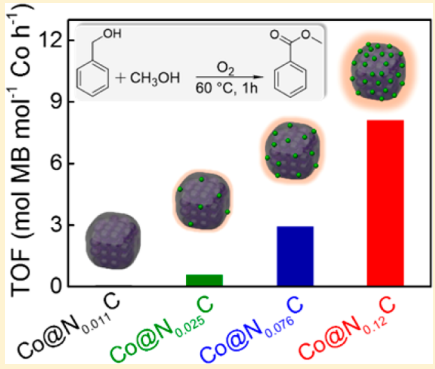

1. INTRODUCTION

Selective oxidation of alcohols is a promising method in green organic synthesis; it can be used to produce aldehydes, acids, acetals and esters.[1−4] We focus here on esters because they are needed as bulk chemicals in large amounts in various fields including the fine chemicals, commercial products, and polymer industries.[5,6] In recent years, noble-metal-based homogeneous catalysts have been developed that can function as mild catalysts to promote the chemical transformation from alcohol to ester.[7−10] However, heterogeneous catalysts are preferred industrially for their low cost and ease of separation and reuse. Therefore, supported noble-metal nanoparticles have also been used to promote the transformation from alcohol to ester. However, neither homogeneous catalysts nor noble-metal nanocatalysts are a preferred choice for the green production of esters. Heterogeneous catalysts based on more abundant transition metals promise a larger potential as low-cost and sustainable heterogeneous catalysts for the selective oxidation of alcohols but currently still suffer from low activity. To improve the catalytic activity of these heterogeneous catalysts, various bases have been introduced into reaction systems to activate the substrate and/or the metal nanoparticles and lower the activation energy of specific reaction steps, thereby improving the final conversions.[11−14] Given the demand for a sustainable and environmentally friendly reaction process with fewer or even zero additives and byproducts, the construction of an environmentally benign base-free oxidation system is highly desirable.[15] Again, further promoting the catalytic activity of the transition-metal nanoparticle-based catalysts should be the most direct approach to meet the requirements of green chemistry.

Cobalt and cobalt oxides are earth-abundant and have been used in many chemical processes, including nitroarene reduction, aerobic oxidation of alcohols and the synthesis of nitriles.[11,16−18] The typical strategy using organic ligands to indirectly control the catalytic performance of cobalt-based nanocatalysts already leaves many opportunities to modify the electronic environment of the Co nanoparticles and boosts their final catalytic activity.[16] Recently, we introduced the concept of a Mott–Schottky photocatalyst to activate the metal sites by using carbon nitride-based semiconductive materials for H_2 generation reactions, hydrogenation reactions and carbon–carbon coupling reactions.[19−21] The manner of activation of the carbon nitride support is analogous to the function of a ligand in homogeneous catalysts, where the electron density at the metal centers can be adjusted by introducing special organic ligands with electron-donating or -accepting groups.[22] As a

Received: October 13, 2016
Published: December 23, 2016

DOI: 10.1021/jacs.6b10710
J. Am. Chem. Soc. 2017, 139, 811–818

heterogeneous version of metal−ligand complexes, the heterojunction of the metal nanoparticle with a semiconductive support is strongly capable of changing the electron density within the metal, as the work function of the electrons at the Schottky barrier is continuous, and the Fermi levels adjust through an effective flow of charges through the metal−support interface. This charging or discharging effect can be much stronger than any ligand effect and finally promotes the activity of metal particles for specific catalytic reactions.[23,24]

Among the majority of semiconductive or semimetallic catalyst supports, carbon-based materials with their adjustable electron structure and chemical stability have prominent advantages in stabilizing metal nanoparticles.[25,26] Nitrogen-doped carbon supports usually serve as general promoters to enhance the catalytic activity of various nanocatalysts for specific reactions.[27,28] In this work, we exploit the fact that moderate to high level of nitrogen dopants allow the modification of the flat band potential (or "nobility") of the carbon simplistically, where more nitrogen creates a more noble support material. In this way, nitrogen-doped carbon/metallic cobalt based heterogeneous catalysts can be constructed and fine-tuned for the efficient and sustainable oxidation of alcohols to esters.[29−31] Herein, we report the construction of an effective Mott−Schottky catalyst system based on nitrogen-rich carbon-coated cobalt nanoparticles (Co@NC) for the base-free oxidation of alcohol to ester under mild conditions. Co@NC samples were prepared via the direct calcination of a mixture of a metal salt, inexpensive organic molecules and graphitic carbon nitride (g-C_3N_4) powder (Figure 1a). Such a simple method proved to be powerful to tune the nitrogen content of carbon supports without extensively disturbing the morphology and content of the Co nanoparticles. The highly integrated structure of the Co@NC dyads with Co nanoparticles encapsulated inside carbon shells enables the construction of a rectifying contact at the Co/NC interface and changes the electron density of the Co nanoparticles. An optimized Co@NC is shown to promote the catalytic oxidation and subsequent cross-esterification of alcohols to esters, which was not observed in the case of bare nitrogen-doped carbon support or pristine carbon-supported Co nanoparticles. The observed activity was found to be 30-times higher than the best current state-of-the-art transition-metal catalyst.

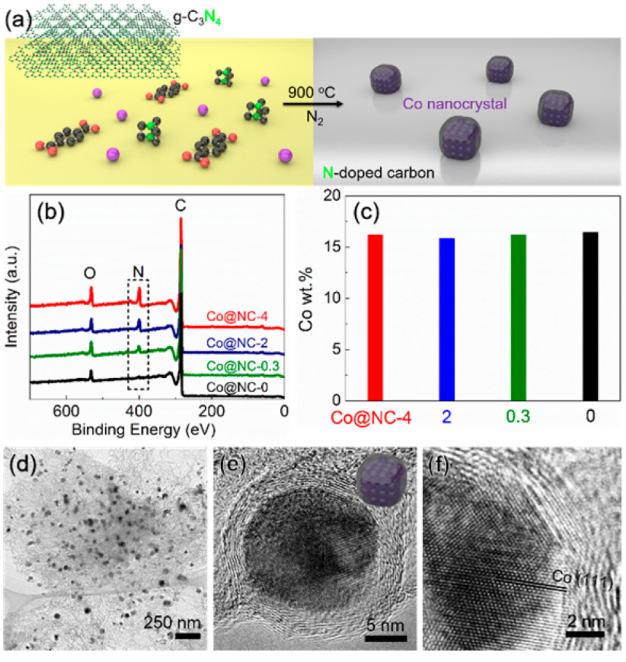

Figure 1. Synthesis and structure of the Co@NC-*x* catalyst. (a) Proposed synthetic protocol for Co@NC from metal−organic precursors (Co^{2+} cations, terephthalic acid and triethylene diamine) and bulk carbon nitride powder. Carbon atoms are black, nitrogen atoms are green, oxygen atoms are red and cobalt atoms are purple. (b) XPS spectra and (c) cobalt contents, as determined by ICP analysis, of the Co@NC-*x* samples (*x*: mass ratios of g-C_3N_4 and metal−organic precursor). Typical (d) TEM and (e, f) HRTEM images of Co@NC-4.

2. EXPERIMENTAL SECTION

Synthesis of g-C_3N_4. Urea was placed in a covered crucible, heated over 4h to 550 °C in air and maintained at this temperature for another 4h. The as-formed yellow solid was ground into a powder for further use.

Synthesis of Co@NC. The homogeneous cobalt-containing precursor solution was prepared by dissolving cobalt nitrate hexahydrate (1.168 g), 1,4-benzenedicarboxylic acid (2.72 g) and triethylene diamine (1.92 g) in 150 mL of dimethylformamide (DMF). Then g-C_3N_4 (0, 1.39, 9.28, 18.56, or 27.84 g for Co@NC-0, Co@NC-0.3, Co@NC-2, Co@NC-4 or Co@NC-6, respectively) was added to the mixed DMF solution under magnetic stirring. After solvent was removed, the green solid powder was transferred to a covered crucible, heated to 900 °C at a rate of 1.5 °C/min under an N_2 atmosphere and maintained at this temperature for 1 h (Figure S1). The as-obtained black solid samples were used for further characterizations and catalytic reactions.

Synthesis of Co@NC-H^+. Fifty milligrams of the as-obtained Co@NC-4 was placed in 10 M HCl solution (50 mL), and the solution was stirred vigorously at 90 °C for 24 h. The obtained black sample was then washed with deionized water and dried at 60 °C for subsequent characterizations and catalytic reaction.

Characterizations. The scanning electron microscopy (SEM) observations were performed on a Nova NanoSEM 450 field emission scanning electron microscope (FEI, USA). The transmission electron microscopy (TEM) and high-resolution transmission electron microscopy (HRTEM) observations were carried out on a JEM-2100F microscope operated at an acceleration voltage of 200 kV. Powder X-ray diffraction patterns (XRD) were recorded on a Bruker D8 Advance X-ray diffractometer equipped with a Cu Kα radiation source (λ = 1.5418 Å) and operated at a scan rate of 6° min^{-1}. TGA was performed on a SDT Q600 thermoanalyzer (DSC-TGA, TA Instruments, USA) under flowing nitrogen; the heating rate was 10 °C min^{-1}. The XPS measurements were conducted on a Kratos Axis Ultra DLD spectrometer using a monochromated Al Kα radiation. The inductively coupled plasma (ICP) measurements were conducted on a PerkinElmer Optima 3300DV (ICP) spectrometer for elemental analysis. Elemental analysis (EA) was carried out on a Vario EL Cube equipped with an M5X analytical balance. Conversions of all substrates were determined via gas chromatography (GC) or gas chromatography−mass spectrometry (GC−MS) analysis.

Oxidative Esterification of Benzyl Alcohol under Base-Free Conditions. Ten milligrams of the catalysts (Co@NC-*x*, 5.5 mol % Co), 4 mL of methanol and benzyl alcohol (0.5 mmol) were added into a 10 mL round-bottom flask. After the flask was purged 3 times with oxygen gas, the mixture was stirred under 1 bar of oxygen at 60 °C for 1 h (or 4, 8, 12 h), followed by natural cooling to room temperature. The reaction temperature was maintained in oil bath. After the catalysts were collected by filtration, the remaining liquid mixture was used directly for GC with a flame ionization detector (FID) and/or for GC−MS analysis.

Experimental Details of Oxidative Esterification of Benzyl Alcohol with Base. Ten milligrams of catalysts (Co@NC-*x*, 5.5 mol % Co), K_2CO_3 (0.1 mmol), 4 mL of methanol and benzyl alcohol (0.5 mmol) were added into a 10 mL round-bottom flask. After the flask

DOI: 10.1021/jacs.6b10710
J. Am. Chem. Soc. 2017, 139, 811−818

was purged 3 times with oxygen, the mixture was stirred under 1 bar of oxygen at 60 °C for 1 h followed by natural cooling to room temperature. The reaction temperature was maintained in oil bath. The catalysts were removed by filtration, and the remaining liquid mixture was used directly for GC analysis with a FID and/or GC−MS analysis.

Quenching Reactions for Catalytic Oxidation of Benzyl Alcohol over the Co@NC Catalyst. Ten milligrams of Co@NC-4 (5.5 mol % Co), KSCN (0.2 mmol) or butylated hydroxytoluene (0.2 mmol) and 4 mL of methanol were placed into a 10 mL round-bottom flask, and the mixtures was stirred at room temperature for 24 h. Then benzyl alcohol (0.5 mmol) was added to the flask. After the flask was purged 3 times with oxygen, the mixture was stirred under 1 bar of oxygen at 60 °C for 12 h followed by natural cooling to room temperature. After the catalysts were collected by filtration, the remaining liquid mixture was used directly for GC analysis with a FID.

Recycling Reaction of Catalyst for Oxidative Esterification of Benzyl Alcohol. The used catalyst was separated by centrifugation and washed with 0.1 M NaOH and pure methanol. The catalyst was then used for the next catalytic reaction.

3. RESULTS AND DISCUSSION

Preparation and Structure of the Co@NC-*x* Catalyst. To enable a larger-scale production of the Co@NC materials for possible use as heterogeneous catalysts, we developed a simple thermal condensation method using a metal salt (exemplified by $Co(NO_3)_2$ here), and low-cost organic molecules (terephthalic acid and triethylene diamine) as the precursors. Graphitic carbon nitride powder (bulk phase), as the main nitrogen source for the formation of nitrogen-rich carbon supports, was then added to the mixed solution of the metal salt and organic molecules in DMF. The solid mixture after the solvent was removed, was carbonized at 900 °C under an N_2 atmosphere (Figure S1). The as-obtained black powder was used directly for further characterizations and catalytic reactions.

A series of Co@NC samples were obtained at 900 °C in an N_2 atmosphere from the mixture of carbon nitride powder and metal−organic ligand precursors with different weight ratios (x = 0, 0.3, 2, 4), where the as-obtained samples were denoted as Co@NC-x, accordingly. Bulk g-C_3N_4 decomposes completely into gaseous, nitrogen-rich fragments at temperatures higher than 680 °C (Figure S2) and acts as a pore template and the main nitrogen source at the same time. Considering the fact that the mixture of cobalt salt and organic molecules could be carbonized into carbon materials at an even lower temperature than 680 °C, we speculated that a confined carbonization process[32,33] on the surface of g-C_3N_4 particles may be a possible path for the formation of pores or a foam-like structure of Co@NC-x. The morphology of the nitrogen-doped carbon supports is a carbon foam, as revealed by the scanning electron microscopy (SEM) observation (Figure S3), and does not change much by adding different amounts of the g-C_3N_4 powder. The X-ray photoemission spectroscopy (XPS) analysis results (Figure 1b) revealed a linear relationship between the nitrogen contents of the carbon support and the amount of the g-C_3N_4 powder added. The real N content of the Co@NC samples was estimated to be between 0.98 and 8.72 wt % for Co@NC-0 and Co@NC-4, respectively, on the basis of elemental analysis results (Table S1). Further increasing the weight ratio between the carbon nitride powder and metal−organic ligand precursor to 6 (for Co@NC-6) or even higher did not result in a greater nitrogen content of Co@NC any further, but resulted only in a lower yield of the catalyst materials.

The XRD patterns (Figure S4) indicate the formation of metallic cobalt and graphitic carbon as the main components of the Co@NC-x samples, and also exclude the coexistence of a detectable amount of crystalline cobalt oxides, nitrides or carbides. Notably, triethylene diamine molecules were required to prevent excessive growth (Figure S5) in all of the Co@NC-x samples. The TEM observations (Figure 1d and S6−S7) indicate that Co nanoparticles in the Co@NC-x samples exhibited a similar mean size between 28 and 30 nm. The contents of Co nanoparticles are all approximately 16 wt % for the Co@NC samples, as demonstrated by ICP analysis (Figure 1c). Again, the involvement of g-C_3N_4 powder did not obviously change the structure and composition of the Co nanoparticles. Furthermore, the HRTEM image of Co@NC-4 (Figure 1e) revealed a highly integrated nanostructure of the layered carbon-coated Co nanoparticle. A lattice spacing of 0.205 nm was observed (Figure 1f), which is attributed to the (111) plane of metallic cobalt. Obviously, the carbon layers act as a shell to protect the metallic Co nanoparticles from aggregation and oxidation during the synthesis process and the following selective oxidation of alcohols. The X-ray absorption near-edge structure (XANES) results (Figure S8) revealed the metallic feature of the Co components in all Co@NC-x samples. The Fourier-transformed X-ray absorption fine structure spectra (Figure S9) further indicated that Co-X (X = C, N, O) bonds in the Co@NC-x samples were negligible.

Catalytic Oxidation of Benzyl Alcohol over the Co@NC-*x* Catalysts. Direct esterification of alcohol under base-free condition as a green and sustainable process requires an efficient catalyst to promote the activation of oxygen molecules and alcohols. As a proof-of-concept application of the Mott−Schottky catalyst, such a model reaction could directly reflect the catalytic activity of the activated Co nanoparticles with a fixed loading amount and constant particles size but different concentrations of nitrogen dopants in the carbon support. Initially, we tested the activity of the catalyst for selective oxidation of benzyl alcohol using O_2 gas as the oxidant under mild and base-free conditions. As shown in Figure 2a, aerobic esterification of benzyl alcohol and methanol could not proceed in the absence of either catalyst (Entry 1, Table S2) or O_2 (Entry 2, Table S2). Only a trace amount of benzyl alcohol was oxidized to benzaldehyde over Co@NC-0 (Entry 3, Table S2). These results reveal that the Co-nanoparticle-based catalysts without the special support could not promote the aerobic esterification of benzyl alcohol in the absence of base under mild conditions, whereas Co@NC-x could considerably prompt the formation of methyl benzoate (MB) under the identical conditions. The catalytic activity of Co@NC-x can be adjusted via tuning the concentration of nitrogen dopants in the carbon support (Entries 4−7, Table S2 and Table S3). Co@NC-0.3 and Co@NC-2 could successfully trigger the esterification of benzyl alcohol and give conversions of 12% and 31%, respectively but with poor selectivity (<52%). The Co@NC-4 catalyst exhibited the best performance among all of the samples tested in this work, giving the highest conversion of benzyl alcohol (58%) and selectivity toward methyl benzoate (77%). Co@NC-6 did not perform better (Entry 7, Table S2 and Entry 5, Table S3) because a further increase of the amount of g-C_3N_4 powder in the precursor did not further elevate the nitrogen content (Table S1). Considering the relatively low yield of Co@NC-6, we used Co@NC-4 as the best-in-class catalyst for the activation of oxygen and alcohol molecules, in all subsequent experiments. All these results indicate the key

DOI: 10.1021/jacs.6b10710
J. Am. Chem. Soc. 2017, 139, 811−818

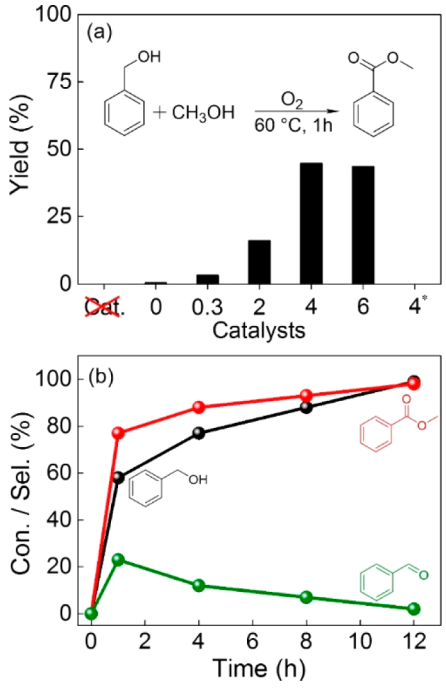

Figure 2. Catalytic oxidation of benzyl alcohol over the Co@NC-*x* catalysts. (a) Yields of methyl benzoate from base-free esterification of benzyl alcohol and methanol over Co@NC-*x* (*x* = 0, 0.3, 2, 4, 6) catalysts. Standard base-free conditions: 0.5 mmol benzyl alcohol, 4 mL of CH3OH, 5.5 mol % Co@NC-*x*, 60 °C, 1 h and 1 bar of O_2; for 4*: 1 bar O_2 was replaced with 1 bar N_2. The conversion and selectivity were determined by gas chromatography (GC). (b) Conversion of benzyl alcohol (black) and selectivity for methyl benzoate (red) and benzaldehyde (green) over Co@NC-4 at different reaction time intervals.

role of the nitrogen-rich carbon support in generating the catalytic activity of Co nanoparticles in Co@NC for the aerobic esterification of alcohols using molecular oxygen.

Further prolonging the reaction time led to a complete conversion of benzyl alcohol to methyl benzoate over Co@NC-4 (Figure 2b and Entries 8−10 of Table S2) with a turnover number (TON) of 18 (Table S4). Removal of the Co nanoparticles from Co@NC-4 via acid etching significantly lowered its catalytic activity, leading to only a trace amount of benzaldehyde formed within 12 h (Figure 3a and Entry 11 of Table S2). Initially, the sample denoted as Co@NC-H^+ was obtained after etching Co@NC-4 with 10 M HCl, leading to a loss of 53% of Co components on the basis of ICP analysis. The residual cobalt particles are mainly those encased in a thicker carbon shell, where the reactant molecule cannot easily contact them (Figure S10) for possible catalytic reactions. Moreover, the involvement of SCN^- ions, which are generally known to poison the metal-Nx/C catalyst in oxygen reduction reactions,[34] could not completely quench the esterification of benzyl alcohol. A conversion of 30% and a selectivity of 21% to methyl benzoate were achieved with Co@NC-4 even in the presence of 40 mol % of KSCN (Figure 3b and Entry 12 of Table S2), indicating much higher tolerance and stability of the presented catalytic system.

In the process of the catalytic reaction, benzaldehyde as the only intermediate product (Figure 2b) further reacts with methanol to give methyl benzoate (Figure 3c and Entry 13 of Table S2). As shown in Figure 3d and Entry 14 of Table S2, the conversion of benzyl alcohol over Co@NC-4 largely decreased after the addition of a free-radical scavenger, butylated hydroxytoluene (BHT). Such a depressed conversion suggests that the reaction in our catalytic system progresses via the superoxide radical anion ($\cdot O_2^-$). Furthermore, the electron paramagnetic resonance (EPR) results obtained using 5,5-dimethyl-1-pyrroline *N*-oxide (DMPO) as the capture agent directly confirmed the formation of $\cdot O_2^-$ radicals during the reaction process (Figure S11). The fact that benzyl acid was not detected through GC−MS (Figure S12) further excluded the formation of free superoxide radical anions in the solution. As depicted in Figure 3e, the absorbed $\cdot O_2^-$ on the surface of Co@NC-4 bound as a polaron with the counterradical in the Co-nanoparticle ensured the high selectivity for methyl benzoate through a tandem process, including the oxidation of benzyl alcohol to benzaldehyde and further dehydrogenative oxidation of the hemiacetal with methanol.[35] The second oxidation must progress via the hemiacetal, because benzaldehyde is not further oxidized by the current catalytic system.

Mott−Schottky Effect on the Catalytic Performance of Co Nanoparticles in Co@NC-*x* Catalysts. Further analysis of the structure (Figure 4) of the Co@NC-*x* catalyst was

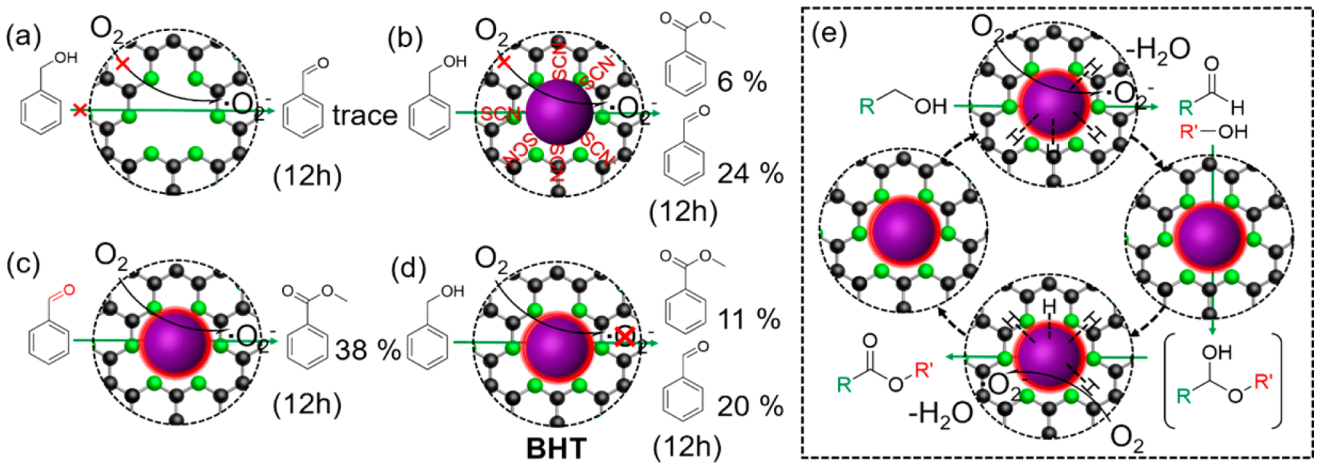

Figure 3. Yields of various products from base-free esterification of benzyl alcohol and methanol (a) over Co@NC-H^+ and over Co@NC-4 in the presence of (b) SCN^- or (d) BHT. (c) Base-free esterification of benzaldehyde and methanol over Co@NC-4. (e) Proposed reaction pathway for aerobic base-free esterification of alcohol over Co@NC-4.

DOI: 10.1021/jacs.6b10710
J. Am. Chem. Soc. 2017, 139, 811−818

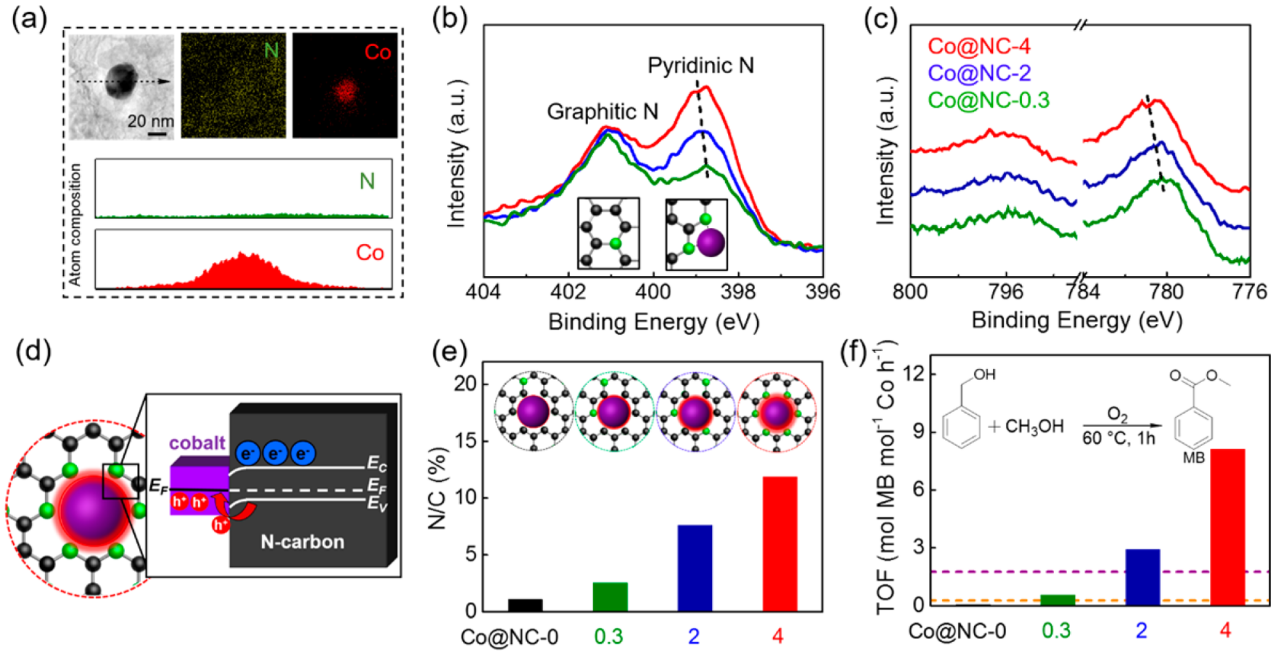

Figure 4. Mott–Schottky effect on the catalytic performance of the Co@NC-*x* catalysts. (a) Nitrogen (green) and cobalt (red) elemental-mapping images and the corresponding line profile of a typical Co@NC-4 sample. (b) N 1s and (c) Co 2p XPS spectra of Co@NC-*x*. (d) Schematic illustration of Mott–Schottky-type contact of Co@NC. (e) The N/C mole ratio of Co@NC-*x* samples as determined by elemental analysis and the corresponding schematic structures (inset of e). (f) TOF values for methyl benzoate (MB) production via aerobic esterification of benzyl alcohol and methanol over Co@NC-*x* in this work and the highest TOF values over a Co-based heterogeneous catalyst with (purple line) or without (orange line) the addition of base reported in the literature (for detailed information, please see Tables S5 and S6).

conducted to collect additional evidence on how the nitrogen-rich carbon support activates the Co nanoparticles for the selective oxidation of benzyl alcohol. The similar morphology (Figure S3) of all Co@NC-*x* samples excludes the obvious effects of the cobalt content (Figure 1c), particle size (Figure S7), and nanostructure of Co nanoparticles and carbon support (Figures S3 and S6) on the final catalytic activity. The significant effect of surface area (Figure S13) on the final catalytic activity was also excluded here because Co@NC-0 with a surface area one-third of that of Co@NC-4 was nearly inert for the base-free aerobic oxidation of alcohols. Elemental-mapping images and the energy-dispersive X-ray spectroscopy (EDS) line-scan profiles (Figure 4a) directly demonstrate the homogeneous distribution of N atoms in the carbon framework. The introduced N atoms are mainly graphitic and pyridinic, as revealed by the N 1s XPS spectra (Figure 4b and Figure S14). Combined with the EXAFS analysis results (Figures S8 and S9), the O 1s XPS spectra with typical peaks centered at 531.5 eV, which is attributed to absorbed oxygen-containing species, further excluded the presence of an obvious amount of cobalt oxide surface layers (typical XPS peak at 529.2 eV) in the Co@NC samples[36,37] (Figure S15). The gradual shifts of typical Co 2p XPS peaks (Figure 4c) to higher energy further indicate the gradually depressed electron density of Co particles in Co@NC-*x* samples with the introduction of more nitrogen dopants. This observation again demonstrated the key role of the Mott–Schottky effect at the interface of the heterojunction in modifying the electron density and thus the final catalytic activity of Co particles.

Theoretical investigation suggested that the electronic structure of carbon framework could be controlled by introducing nitrogen atoms to lower the valence band and elevate the conduction band.[38−40] Note that the type of nitrogen-rich carbon, as an ambipolar support[41,42] acting in the metal/NC heterojunction, is mainly dominated by the work functions of two components. Because the work function of Co is located close to that of N-doped carbon, the flow of electrons (Figure 4d) sensitively depends on the nitrogen content and the structure. Nitrogen-rich carbon with a relatively higher flat band potential (or work function) than that of metallic Co materials, will accept electrons from Co nanoparticles until their Fermi level reaches equilibrium. This electron transfer is described as the Mott–Schottky effect in solid-state physics. Such a Schottky barrier will obviously result in an electron redistribution at the interface of cobalt and nitrogen-doped carbon and enrich the positive charges on the side of metallic cobalt. The more oxidative area thus forms on the side of the Co nanoparticles accordingly. Typical XPS peaks (Figure 4b,c) of pyridinic nitrogen and Co gradually shift to higher binding energy values as the nitrogen content (Figure 4e) in Co@NC-*x* increases from Co@NC-0.3 via Co@NC-2 to Co@NC-4. The fact that the electron density at the nitrogen decreases (according to the XPS results, the binding energy increased gradually) with increasing nitrogen content unambiguously supports the electron transfer over the Mott–Schottky heterojunction at the interface of metallic cobalt and carbon, as depicted in Figure 4d. We note that the electron-rich and electron-deficient areas induced by the Mott–Schottky contact are only several nanometers thick and are located at the interface, because opposite charges attract each other and are also bound to each other as a cross-interface polaron.

Besides the oxidation of the substrate molecules, further oxidative deprotonation of the H-metal intermediates to regenerate the catalytically active surface of metal nanocatalysts is of key importance to accelerate the whole reaction process.[43] Various bases were added in previous works to facilitate such a

DOI: 10.1021/jacs.6b10710
J. Am. Chem. Soc. 2017, 139, 811–818

Table 1. Co@NC Catalyzed Cross-Esterification of Substituted Aromatic and Aliphatic Alcohol

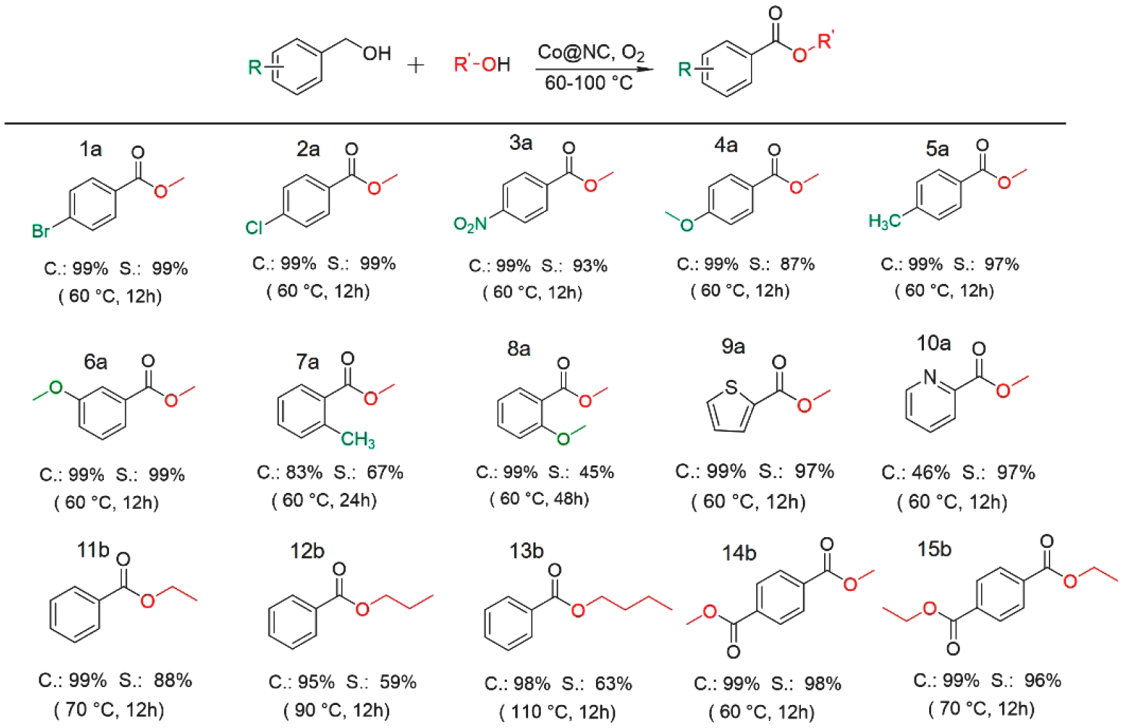

[a]Reaction conditions a: 0.5 mmol substrates, 4 mL of CH_3OH, 5.5 mol % Co catalyst, 60 °C, 12 h and 1 bar O_2. Condition b: 0.1 mmol substrates, 4 mL of aliphatic alcohol, 40 mg of Co@NC-4, 70−110 °C, 12 h and 1 bar O_2. The conversion (*C*) and selectivity (*S*) were determined by GC and/or GC−MS.

deprotonation process. In our case, the electron-poor Co nanoparticles are sufficiently strong to attract and activate O_2 for the further removal of protons from the proposed Co−H intermediates.

More importantly, the nitrogen-doped carbon could also act as built-in and "strengthened" Lewis base to accelerate the deprotonation process. Further temperature-programmed desorption (TPD) analysis results (Figure S16) of typical samples, where CO_2 is used as the probe molecule, directly confirmed the formation of novel and strong basic sites in the Co@NC-*x* dyads, because of the enhanced electron density of nitrogen-doped carbon induced by the Mott−Schottky effect.

As a result, the Co@NC-*x*-based Mott−Schottky catalysts not only boost the oxidative power of the Co-nanoparticles, but also enable the reaction to proceed in the absence of bases to constitute an overall mild and additive-free catalytic system. As the best catalyst in this work, Co@NC-4 offers a high turnover frequency (TOF) of 8.12 mol methyl benzoate mol^{-1} Co h^{-1} for base-free oxidation of benzyl alcohol. Such a TOF value is an order of magnitude higher than the values (orange line in Figure 4f) reported for current transition-metal-based heterogeneous catalysts in base-free systems (Table S5). Furthermore, it is superior to those (purple line in Figure 4f) obtained in base-containing catalytic systems (Table S6).[11−13]

Co@NC Catalyzed Cross-Esterification of Substituted Aromatic and Aliphatic Alcohols. To investigate the general applicability of Co@NC-4, various substituted benzyl alcohols with both electron-withdrawing (Br, Cl, NO_2) and electron-donating (OCH_3 and CH_3) functional groups were oxidized under standard conditions. The Co@NC-4 sample generally gave high conversions (99%) of these substituted benzyl alcohols and selectivity (>87%) toward corresponding methyl esters under base-free conditions (**1a**−**5a** of Table 1). The preadsorption of the diverse substrates on the surface of Co@NC-4 was significantly modified by the substitution and the steric arrangement of functional group. This hypothesis can be partially confirmed by the presence of a steric effect in the *para*, *meta* and *ortho* isomers of methoxybenzyl alcohols with a reactivity trend of *para* (**4a** of Table 1) < *meta* (**6a** of Table 1). The moderate selectivity (<57%) for ortho-substituted methyl benzoate (Entries 1 and 5, Table S7) demonstrates the blocking effect of these functional groups on the esterification reaction of the corresponding alcohols. The yields of the ortho-substituted methyl benzoate can be optimized by longer reaction times (**7a**−**8a** of Table 1) or adding more catalysts (Entries 4 and 7 of Table S7). Even heterocyclic alcohols including 2-thiophenemethanol (**9a**, Table 1) and 2-pyridinemethanol (**10a** of Table 1) could be oxidized over Co@NC-4 to their corresponding esters with good conversion and high selectivity. The advantages of Co@NC-4 over noble-metal-based catalysts with respect to being more resistant against "poisoning" by N or S atoms are clearly demonstrated. The aerobic esterification of benzyl alcohol with other aliphatic alcohols, including ethanol, propanol and butanol, also proceeds smoothly in the same base-free catalytic system, further expanding the scope of the synthesis of esters from methyl to other alkyl esters (**11b**−**13b** in Table 1 and Table S8). All these results indicate the high chemoselectivity and functional-group tolerance of Co@NC-4 for base-free aerobic esterification of alcohols using molecular oxygen.

Dimethyl terephthalate and diethyl terephthalate are two main monomers for the polymerization of polyethylene terephthalate (PET), one of most important engineering plastics.[6,44] The aerobic esterification of 1, 4-benzenedimethanol and methanol/ethanol produced dimethyl terephthalate (**14b** in Table 1)/diethyl terephthalate (**15b** in Table 1) in the

DOI: 10.1021/jacs.6b10710
J. Am. Chem. Soc. 2017, 139, 811−818

highest conversions (99%) and selectivity (>96%) over Co@NC-4 under base-free conditions. Such a green and efficient catalytic protocol offers new possibilities for the production of industrially relevant compounds and intermediates in a sustainable manner.

Reusability of Co@NC. We also examined the stability and reusability of the Co@NC-4 catalyst by recovering the used catalyst for further characterizations and catalytic reactions. The Co@NC-4 catalyst could be reused at least three times (Figure S17) with only a slight attenuation of activity, which was mainly attributed to the loss of catalyst after centrifugation. The structure of the used Co@NC-4 catalyst was not visibly changed as demonstrated by the XRD and TEM analysis results (Figure S18). Moreover, a deprotonation process, where the used Co@NC-4 catalyst was washed with 0.1 M NaOH solution, was carried out to ensure its activity, again suggesting the deprotonation process is the key step in the whole aerobic esterification reaction of benzyl alcohol over the Co@NC heterogeneous catalyst.

4. CONCLUSIONS

We report the *de novo* design of a heterogeneous catalytic systems to boost the activity of a transition-metal nanocatalyst by creating a Mott−Schottky interface at metal/nitrogen-doped carbon. Nitrogen-rich carbon shells with controllable concentration of nitrogen dopants were used to adjust the electron density within the as-embedded cobalt nanoparticles via enhancing the electron transfer over the Schottky barrier; this electron transfer substantially enhanced the final activity of the cobalt/carbon dyad for aerobic esterification of alcohols to the corresponding esters using molecular oxygen. Because the synthesis of Co@NC-*x* catalysts from simple organic molecules, inorganic metal salts and g-C_3N_4 powder is easily scaled up, we expect a more general applicability of such a series of transition-metal/nitrogen-rich carbon-based nanocatalysts for specific catalytic reactions. Most importantly, Mott−Schottky electron-transfer-induced enhancement of the catalytic activity of metallic nanoparticles could be used as a general principle to design more efficient and sustainable heterogeneous catalysts for energy storage, organic synthesis and synthesis of fine chemicals.

■ ASSOCIATED CONTENT

Supporting Information

The Supporting Information is available free of charge on the ACS Publications website at DOI: 10.1021/jacs.6b10710.

Experimental details, more characterization results, and detailed discussions (PDF)

■ AUTHOR INFORMATION

Corresponding Author

*xinhaoli@sjtu.edu.cn (X.-H. Li)

ORCID

Hui Su: 0000-0002-2257-4342

Notes

The authors declare no competing financial interest.

■ ACKNOWLEDGMENTS

This work was supported by National Basic Research Program of China (2013CB934102), National Natural Science Foundation of China (21331004, 21301116, 21673140), SJTU-UM joint grant, SJTU-MPI partner group, Shanghai Basic Research Program (16JC1401600), Shanghai Eastern Scholar Program and Shanghai Rising-Star Program (16QA1402100).

■ REFERENCES

(1) Enanche, D. I.; Edwards, J. K.; Landon, P.; Espria, B. S.; Carley, A. F.; Herzing, A. A.; Watanabe, M.; Kiely, C. J.; Knight, D. W.; Hutching, G. J. *Science* **2006**, *311*, 362−365.

(2) Kaizuka, K.; Miyamura, H.; Kobayashi, S. *J. Am. Chem. Soc.* **2010**, *132*, 15096−15098.

(3) Gunanathan, C.; Shimon, L. J. W.; Milstein, D. *J. Am. Chem. Soc.* **2009**, *131*, 3146−3147.

(4) Liu, C.; Wang, J.; Meng, L. K.; Deng, Y.; Li, Y.; Lei, A. W. *Angew. Chem., Int. Ed.* **2011**, *50*, 5144−5148.

(5) Nielsen, M.; Junge, H.; Kammer, A.; Beller, M. *Angew. Chem., Int. Ed.* **2012**, *51*, 5711−5713.

(6) Lu, R.; Lu, F.; Chen, J. Z.; Yu, W. Q.; Huang, Q. Q.; Zhang, J. J.; Xu, J. *Angew. Chem., Int. Ed.* **2016**, *55*, 249−253.

(7) Bai, X. F.; Ye, F.; Zheng, L. S.; Lai, G. Q.; Xia, C. G.; Xu, L. W. *Chem. Commun.* **2012**, *48*, 8592−8594.

(8) Zhang, J.; Leitus, G.; David, Y. B.; Milstein, D. *J. Am. Chem. Soc.* **2005**, *127*, 10840−10841.

(9) Gowrisankar, S.; Neumann, H.; Beller, M. *Angew. Chem., Int. Ed.* **2011**, *50*, 5139−5143.

(10) Liu, C.; Tang, S.; Lei, A. W. *Chem. Commun.* **2013**, *49*, 1324−1326.

(11) Jagadeesh, R. V.; Junge, H.; Pohl, M. M.; Radnik, J.; Brückner, A.; Beller, M. *J. Am. Chem. Soc.* **2013**, *135*, 10776−10782.

(12) Zhou, Y. X.; Chen, Y. Z.; Cao, L.; Lu, J. L.; Jiang, H. L. *Chem. Commun.* **2015**, *51*, 8292−8295.

(13) Xiao, Q.; Liu, Z.; Bo, A.; Zavahir, S.; Sarina, S.; Bottle, S.; Riches, J. D.; Zhu, H. Y. *J. Am. Chem. Soc.* **2015**, *137*, 1956−1966.

(14) Zope, B. N.; Hibbitts, D. D.; Neurock, M.; Davis, R. J. *Science* **2010**, *330*, 74−78.

(15) Zhong, W.; Liu, H. L.; Bai, C. H.; Liao, S. J.; Li, Y. W. *ACS Catal.* **2015**, *5*, 1850−1856.

(16) Westerhaus, F. A.; Wienhöfer, G.; Pohl, M. M.; Radnik, J.; Surkus, A. E.; Rabeah, J.; Junge, K.; Junge, H.; Nielsen, M.; Brückner, A.; Beller, M. *Nat. Chem.* **2013**, *5*, 537−543.

(17) Jagadeesh, R. V.; Junge, H.; Beller, M. *Nat. Commun.* **2014**, *5*, 4123.

(18) Zhu, J. J.; Kailasam, K.; Fischer, A.; Thomas, A. *ACS Catal.* **2011**, *1*, 342−347.

(19) Cai, Y. Y.; Li, X. H.; Zhang, Y. N.; Wei, X.; Wang, K. X.; Chen, J. S. *Angew. Chem., Int. Ed.* **2013**, *52*, 11822−11825.

(20) Gong, L. H.; Cai, Y. Y.; Li, X. H.; Zhang, Y. N.; Su, J.; Chen, J. S. *Green Chem.* **2014**, *16*, 3746−3751.

(21) Li, X. H.; Baar, M.; Blechert, S.; Antonietti, M. *Sci. Rep.* **2013**, *3*, 1743−1749.

(22) Li, X. H.; Antonietti, M. *Chem. Soc. Rev.* **2013**, *42*, 6593−6604.

(23) Li, X. H.; Cai, Y. Y.; Gong, L. H.; Fu, W.; Wang, K. X.; Bao, H. L.; Wei, X.; Chen, J. S. *Chem. - Eur. J.* **2014**, *20*, 16732−16737.

(24) Li, X. H.; Wang, X. C.; Antonietti, M. *Chem. Sci.* **2012**, *3*, 2170−2174.

(25) Gao, Y. J.; Ma, D.; Hu, G.; Zhai, P.; Bao, X. H.; Zhu, B.; Zhang, B. S.; Su, D. S. *Angew. Chem., Int. Ed.* **2011**, *50*, 10236−10240.

(26) Liu, R.; Mahurin, S. M.; Li, C.; Unocic, R. R.; Idrobo, J. C.; Gao, H. J.; Pennycook, S. J.; Dai, S. *Angew. Chem., Int. Ed.* **2011**, *50*, 6799−6802.

(27) Hardin, W. G.; Mefford, J. T.; Slanac, D. A.; Patel, B. B.; Wang, X. Q.; Dai, S.; Zhao, X.; Ruoff, R. S.; Johnston, K. P.; Stevenson, K. J. *Chem. Mater.* **2014**, *26*, 3368−3376.

(28) Mefford, J. T.; Rong, X.; Abakumov, A. M.; Hardin, W. G.; Dai, S.; Kolpak, A. M.; Johnston, K. P.; Stevenson, K. J. *Nat. Commun.* **2016**, *7*, 11053.

(29) Wei, D. C.; Liu, Y. Q.; Wang, Y.; Zhang, H. L.; Huang, L. P.; Yu, G. *Nano Lett.* **2009**, *9*, 1752−1758.

DOI: 10.1021/jacs.6b10710
J. Am. Chem. Soc. 2017, 139, 811−818

(30) Deng, D. H.; Novoselov, K. S.; Fu, Q.; Zheng, N. F.; Tian, Z. Q.; Bao, X. H. *Nat. Nanotechnol.* **2016**, *11*, 218−230.
(31) Zhou, Y. K.; Neyerlin, K.; Olson, T. S.; Pylypenko, S.; Bult, J.; Dinh, H. N.; Gennett, T.; Shao, Z. P.; O'Hayre, R. *Energy Environ. Sci.* **2010**, *3*, 1437−1446.
(32) Deng, J.; Ren, P. J.; Deng, D. H.; Bao, X. H. *Angew. Chem., Int. Ed.* **2015**, *54*, 2100−2104.
(33) Wang, X. Q.; Dai, S. *Angew. Chem., Int. Ed.* **2010**, *49*, 6664−6668.
(34) Wang, Q.; Zhou, Z. Y.; Lai, Y. J.; You, Y.; Liu, J. G.; Wu, X. L.; Terefe, E.; Chen, C.; Song, L.; Rauf, M.; Tian, N.; Sun, S. G. *J. Am. Chem. Soc.* **2014**, *136*, 10882−10885.
(35) Whittaker, A. M.; Dong, V. M. *Angew. Chem., Int. Ed.* **2015**, *54*, 1312−1315.
(36) Lv, L. B.; Ye, T. N.; Gong, L. H.; Wang, K. X.; Su, J.; Li, X. H.; Chen, J. S. *Chem. Mater.* **2015**, *27*, 544−549.
(37) Su, H.; Wang, H. H.; Zhang, B.; Wang, K. X.; Li, X. H.; Chen, J. S. *Nano Energy* **2016**, *22*, 79−86.
(38) Wang, C.; Qiao, L.; Qu, C. Q.; Zheng, W. T.; Jiang, Q. *J. Phys. Chem. C* **2009**, *113*, 812−818.
(39) Xiang, H. J.; Huang, B.; Li, Z. Y.; Wei, S. H.; Yang, J. L.; Gong, X. G. *Phys. Rev. X* **2012**, *2*, 011003.
(40) Wang, X. R.; Li, X. L.; Zhang, L.; Yoon, Y.; Weber, P. K.; Wang, H. L.; Guo, J.; Dai, H. J. *Science* **2009**, *324*, 768−771.
(41) Zhang, Y. J.; Antonietti, M. *Chem. Asian J.* **2010**, *5*, 1307−1311.
(42) Schiros, T.; Nordlund, D.; Pálová, L.; Prezzi, D.; Zhao, L. Y.; Kim, K. S.; Wurstbauer, U.; Gutiérrez, C.; Delongchamp, D.; Jaye, C.; Fischer, D.; Ogasawara, H.; Pettersson, L. G. M.; Reichman, D. R.; Kim, P.; Hybertsen, M. S.; Pasupathy, A. N. *Nano Lett.* **2012**, *12*, 4025−4031.
(43) Sarina, S.; Bai, S.; Huang, Y. M.; Chen, C.; Jia, J. F.; Jaatinen, E.; Ayoko, G. A.; Bao, Z.; Zhu, H. Y. *Green Chem.* **2014**, *16*, 331−341.
(44) Pang, J. F.; Zheng, M. Y.; Sun, R. Y.; Wang, A. Q.; Wang, X. D.; Zhang, T. *Green Chem.* **2016**, *18*, 342−359.

DOI: 10.1021/jacs.6b10710
J. Am. Chem. Soc. 2017, 139, 811−818